Large *Q* Factor with Very Small Whispering-Gallery-Mode Resonators

Nirmalendu Acharyya[1,2] and Gregory Kozyreff[2,*]

[1]*Max-Born-Institut für Nichtlineare Optik und Kurzzeitspektroskopie, D-12489 Berlin, Germany*
[2]*Optique Nonlinéaire Théorique, Université libre de Bruxelles (U.L.B.), CP 231, Campus de la Plaine, 1050 Bruxelles, Belgium*

Efficient microresonators simultaneously require a large quality factor Q and a small volume V. However, the former is ultimately limited by bending losses, the unavoidable radiation of energy of a wave upon changing direction of propagation. Such bending losses increase exponentially as V decreases and eventually result in a drop of Q. Therefore, circular cavities are generally designed with radii that are much larger than the optical wavelength. The same leakage of energy by radiation limits the sharpness of bends in photonic integrated circuits. In this paper, we present a way to reduce bending losses in circular microresonators. The proposed scheme consists of one or more external dielectric rings that are concentric with the cavity. These rings alter the field outside the cavity where radial oscillations set in and thus control the far-field radiation. As a result, the Q factor can be increased by several orders of magnitude while keeping a small cavity volume.

I. INTRODUCTION

Whispering-gallery-mode (WGM) resonators occupy a place of choice in experiments and devices where enhanced light-matter interaction is required. The reason why they attract interest in both fundamental and applied research is that WGMs can have a very long lifetime, measured by the quality factor Q, while occupying a small volume V [1,2]. This makes them extremely sensitive to changes in their environment [3–5] and, hence, especially interesting as biosensors [6–12]. Indeed, through linear processes, the detection of single nanoparticles or molecules the size of a protein or a virus has been experimentally demonstrated [13–15]. Furthermore, a similar detection limit in terms of mass has been reached, but with a set of molecules of much lower molecular weight (<500 Da) using nonlinear optics [16,17]. Next to sensing, WGMs are found to be particularly efficient nonlinear optical sources: lasers [18–20], optical parametric oscillators [21], second-harmonic [22], Raman [23], and third-harmonic sources [24], and, in recent years, frequency combs [25–28]. Regarding phase matching, it was realized [29,30], and later experimentally confirmed [31–33], that the usual conservation of linear momentum gives way to conservation of angular momentum in WGM resonators and that the laws of composition of angular momentum in quantum mechanics apply. Finally, WGM resonators can be used to investigate quantum-cavity electrodynamics

in the strong-coupling regime [34–36] and hold potential as high-quality optical quantum sources [37]. In relation to linear light-matter interaction, an appropriate figure of merit is the Purcell factor $\mathcal{P} = 6\pi Q/(k_r^3 V)$, where k_r is the real part of the wave number in vacuum. Indeed, $\mathcal{P}$ characterizes cavity-induced changes not only in emission but also in scattering by particles, both in the quantum and classical limits [38]. As a general rule, therefore, the optimization of WGM resonators rests on maximizing Q while keeping V as small as possible.

In large cavities, the quality factor is limited by parasitic absorption and scattering. By minimizing these losses using state-of-the fabrication techniques, Q factors in the order of 10^{11} have been demonstrated [39], while values in excess of 10^6 have been reached in various photonic integrated platforms [40–45]. However, this is no longer true as the cavity radius R becomes smaller than about ten wavelengths. Indeed, radiation losses associated with the bending of light trajectories increase exponentially with curvature. They are therefore the main physical obstacle to reducing V while preserving Q.

In this paper, we propose a general procedure to reduce bending losses, which can readily be implemented with existing technologies. It consists of surrounding the circular cavity with properly designed concentric dielectric shells. These give control to the far-field amplitude and, hence, the radiation losses of the WGMs. The more external shells there are in the external structure, the stronger the reduction of bending losses that can be obtained, with no apparent limit. As an example, we show an increase

*gkozyref@ulb.ac.be

of the Q factor from 15 000 to 125 000, 600 000, and 2.5×10^6 with one, two, or three external rings, respectively (here and from now on we restrict our attention to the radiative part of the Q factor). In another extreme case, we consider a WGM with orbital number $\nu = 5$ and vacuum wavelength $\lambda = 1.45 \ \mu$m in a cavity with $R = 1 \ \mu$m only. Starting from an initial quality factor $Q = 12.3$, we obtain $Q \approx 4699$ by adding five external shells, while keeping the WGM entirely within the cavity. The strongest suppression of radiation is generally obtained when the innermost external shell is at the transition where the WGM field switches between exponential (near field) and undulatory (far-field) behavior. Conversely, if desired, the external structure can drastically enhance radiation losses and decrease Q. Hints that radiation losses could be controlled by such a structure were found by an analytical theory in the limit of large R with a single outer shell [46]. Here, we provide a complete theory that remains valid for small R and that applies to any number of external shells. Previous authors have considered geometries that at first sight appear similar to what is considered here [47–51]. (Note, for proper comparison, that the field circulates in the external ring in Ref. [49].) However, the present scheme is different in some fundamental aspects, which explains why the enhancement in Q reported here is several orders of magnitudes larger than in previous works: an enhancement factor of, at most, between 2 and 10 in [48,50] compared to more than 350 in some examples discussed here. In Refs. [47–51], the cavity is coupled to an external curved waveguide, which effectively increases the radius of the ring. By contrast, the external rings considered here are too thin to act as waveguides and the field remains entirely confined inside the cavity. When it contains many shells, the present configuration becomes closer in spirit to Bragg fibers [52,53]. However, we consider photons that circulate in a cavity rather than propagating along the axis of a Bragg fiber. In addition, in the optimal configuration, the first ring is always in the evanescent zone of the cavity and not in the radiation zone, a consideration that is evidently absent in the study of Bragg fibers.

II. THEORY

An analytical understanding of the radiation of a WGM resonator embedded in such a dielectric "sarcophagus" can be obtained in two dimensions (2D). In this framework, the knowledge of the electromagnetic field is entirely encoded in just one of its components, $\psi = E_z$ for transverse electric (TE) modes or $\psi = H_z$ for transverse magnetic (TM) modes. In an annulus defined by $r_{j-1} < r < r_j$, of refractive index n_j, the general form of ψ is as follows:

$$\psi = \left[a_j J_\nu(n_j kr) + b_j Y_\nu(n_j kr) \right] e^{i\nu\theta - ikct}, \qquad (1)$$

where r and θ are the usual polar coordinates, c is the speed of light in vacuum, J_ν and Y_ν are Bessel functions

of the first and second kind [54], and k is the complex wave number. At surfaces of discontinuity of the refractive index, both ψ and either $\partial\psi/\partial r$ (TE) or $n^{-2}\partial\psi/\partial r$ (TM) are continuous. These continuity relations can be expressed as follows:

$$\begin{pmatrix} a_{j-1} \\ b_{j-1} \end{pmatrix} = S_j \begin{pmatrix} a_j \\ b_j \end{pmatrix}, \qquad (2)$$

where the S_j are 2×2 matrices containing combinations of Bessel functions evaluated at appropriate interfaces (see the Appendix). By iterating the process, one may link the innermost and outermost coefficients of Eq. (1), giving

$$\begin{pmatrix} a_0 \\ 0 \end{pmatrix} = S(k) \begin{pmatrix} a_N \\ ia_N \end{pmatrix}, \qquad (3)$$

with $S = S_1 S_2 \ldots S_N$. Above, we have imposed constraints on the combinations of Bessel functions near the origin and in the outermost region, in order to avoid divergence as $r \to 0$ and to impose proper radiation conditions in the far field. The second component of Eq. (3) directly yields the following characteristic equation:

$$S_{21}(k) + iS_{22}(k) = 0, \qquad (4)$$

which has complex roots of the form $k = k_r - ik_i$, from which the quality factor can be deduced as $Q = k_r/(2k_i)$. It rapidly becomes intractable to study Q by direct resolution of Eq. (4) for each choice of geometrical parameter set $\{r_j\}$ as the number of outer rings increases. However, our aim here is to study the effect of the external structure on the radiation properties of the internal one, i.e., to compare k with the complex wave number $k^c = k_r^c - ik_i^c$ of the bare cavity. The latter is easier to compute, as it solves a simpler equation. Moreover, in the situations of interest, k_i^c is by hypothesis not so small that it requires special numerical care. As the innermost layers of the whole guiding structure make up the bare cavity, we may write S in Eq. (3) as $S = S^c S^s$, where S^c and S^s correspond to the cavity and the radiation-shielding structure, respectively. By analogy with the above, k^c satisfies the following simpler equation:

$$S_{21}^c(k^c) + iS_{22}^c(k^c) = 0. \qquad (5)$$

With $k_i^c \ll k_r^c$, we must have either that, to leading order, $|S_{21}^c(k_r^c)| \ll 1$ and $S_{22}^c(k_r^c) = 0$ or that $S_{21}^c(k_r^c) = 0$ and $|S_{22}^c(k_r^c)| \ll 1$. If the cavity is a simple disk, then it is easy to check that $S_{22}^c(k_r^c) = 0$ is precisely the sought-after characteristic equation. For more complicated geometries, we find that this is still the case. This can be traced back to the fact that S_{22}/S_{21} is on the order of $Y_\nu(n_1 kr_1)/J_\nu(n_1 kr_1)$, which is a rapidly increasing function of ν [54]. Hence, a complex resonance of the bare cavity is approximately

given by the following equation:

$$S_{22}^c(k_r^c) = 0, \quad k_i^c \approx -S_{21}^c(k_r^c)/S_{22}'^c(k_r^c), \quad (6)$$

where the prime denotes a derivative. In the situations of interest here, in which ν is not very large, finding the root of $S_{22}^c(k_r)$ does not pose a numerical challenge (for a large-ν treatment, see Ref. [46]). Next, with $S = S^c S^s$, Eq. (4) yields the following:

$$S_{21}^c \left(S_{11}^s + iS_{12}^s\right) + S_{22}^c \left(S_{21}^s + iS_{22}^s\right) = 0. \quad (7)$$

Focusing on the solutions that correspond to perturbed modes of the bare cavity, we note that $k = k_r^c + \Delta k$, with $|\Delta k| \ll k_r^c$. Expanding Eq. (7) near k_r^c and exploiting Eq. (6), we obtain the following:

$$\Delta k \approx - \left[\frac{S_{21}^c \left(S_{11}^s + iS_{12}^s\right)}{S_{22}'^c \left(S_{21}^s + iS_{22}^s\right)} \right] \approx -ik_i^c \left[\frac{S_{11}^s + iS_{12}^s}{S_{22}^s - iS_{21}^s} \right], \quad (8)$$

where the elements on the right-hand side are evaluated at the known value k_r^c. Since $\Delta k = k_r - k_r^c - ik_i$, the change in quality factor that results from the external structure is found to be as follows:

$$\left(\frac{Q}{Q^c}\right)^{-1} = \frac{k_i}{k_i^c} \approx \text{Re} \left[\frac{S_{11}^s \left(k_r^c\right) + iS_{12}^s \left(k_r^c\right)}{S_{22}^s \left(k_r^c\right) - iS_{21}^s \left(k_r^c\right)} \right]. \quad (9)$$

The advantage of the above expression is that it explicitly yields the ratio Q/Q^c without the need to solve the characteristic equation of the complete geometry. It proves to be extremely accurate for values of the orbital number $\nu > 10$ (see Figs. 1–3). Even for $\nu = 5$, it predicts the enhancement of Q to within 15%. There have been a few previous works (see [46] and references therein) in which losses in the asymptotic cases of large circular orbital number ν have been estimated. However, an analytical formula such as Eq. (9), which is nearly exact, has never been presented. The provided formula is very useful, particularly to optimize a shield with many shells, where a numerical resolution of the characteristic equation is laborious. It enables us to circumvent the problems of solving the transcendental equation and merely requires evaluation of the formula for various shield parameters.

The above analysis suggests a simple layer-by-layer design strategy. Starting from the bare cavity, one first considers a single outside shell with inner and outer radii r_a and $r_a' = r_a + d_a$. It is a straightforward matter to optimize the right-hand side of Eq. (9) with respect to only two parameters, r_a and d_a. The greatest single-step enhancement is usually seen with this first outer shell. While several local maxima in the gain Q/Q^c are found (see Fig. 1), the global maximum is typically found near the turning point nR, where the
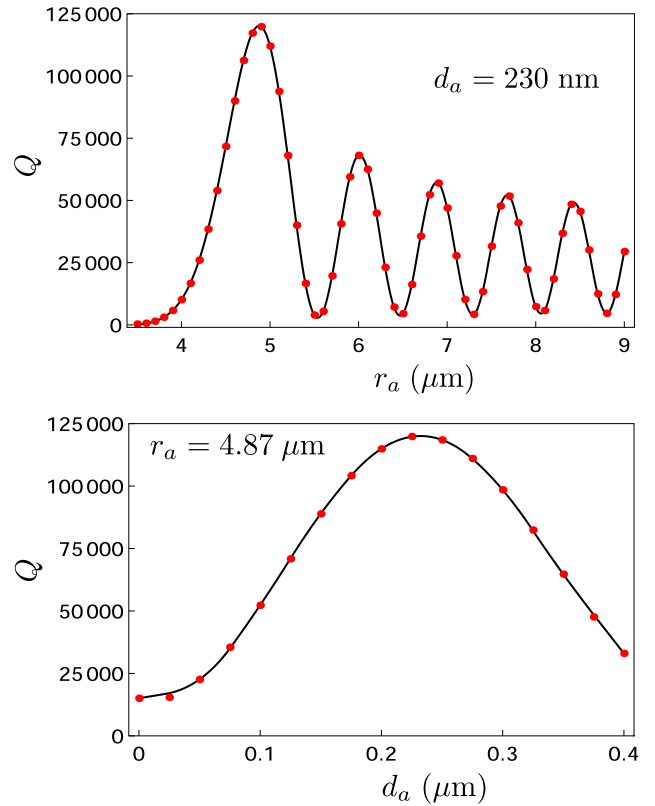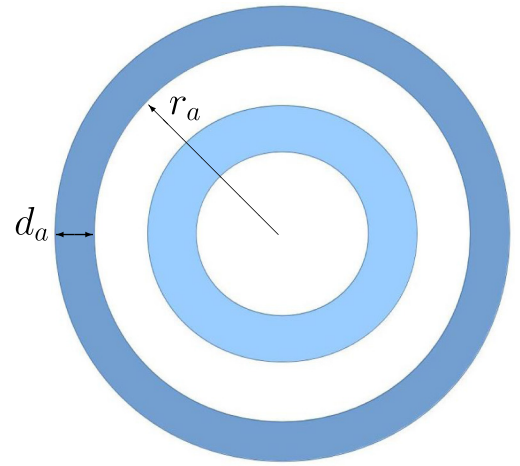

FIG. 1. The radiation quality factor in the presence of a single outer shell for a cavity of radii $r_1 = 2.5$ μm and $r_2 = 3.2$ μm. The refractive index in the cavity and shell, $n = 1.65$; in other regions, $n = 1$. We consider a TE mode with $\nu = 22$ ($\lambda \sim 1.26$ μm). Without a shell, $Q = Q^c \approx 15\,000$. The red dots show the numerical solution of Eq. (4) and the solid lines refer to Eq. (9).

spatial field distribution switches from exponential to oscillating. Subsequent improvements are then achieved by optimizing the parameters of a second shell structure, followed by a third one, etc. To demonstrate this procedure, we first consider an Al_2O_3 ring cavity (refractive
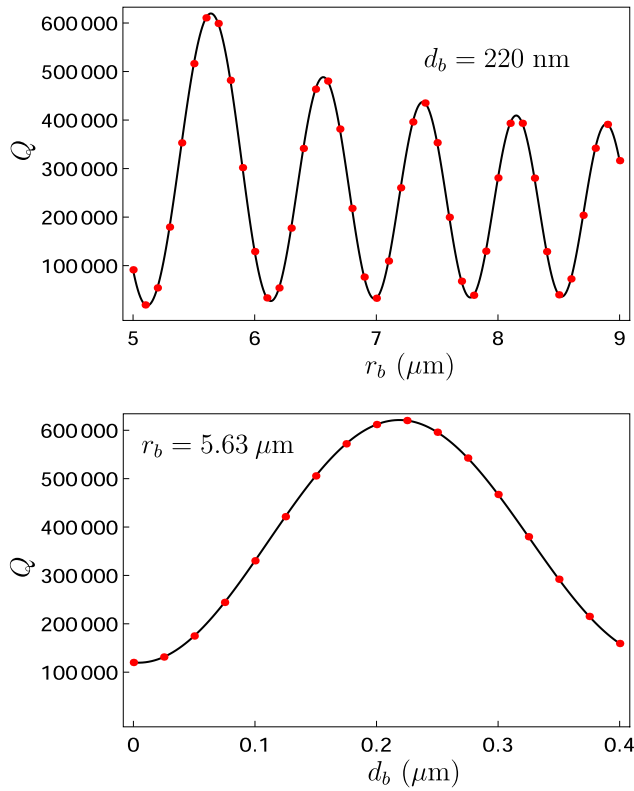
FIG. 2. The Q factor for $\nu = 22$ with two concentric external shells and the same parameters as in Fig. 1. The first concentric shell inner radius and radial thickness are $r_a = 4.87\ \mu$m and $d_a = 0.23\ \mu$m, respectively. Top: Q vs the second shell inner radius r_b with the radial thickness fixed at $d_b = 0.22\ \mu$m. Bottom: Q vs d_b, with $r_b = 5.63\ \mu$m.
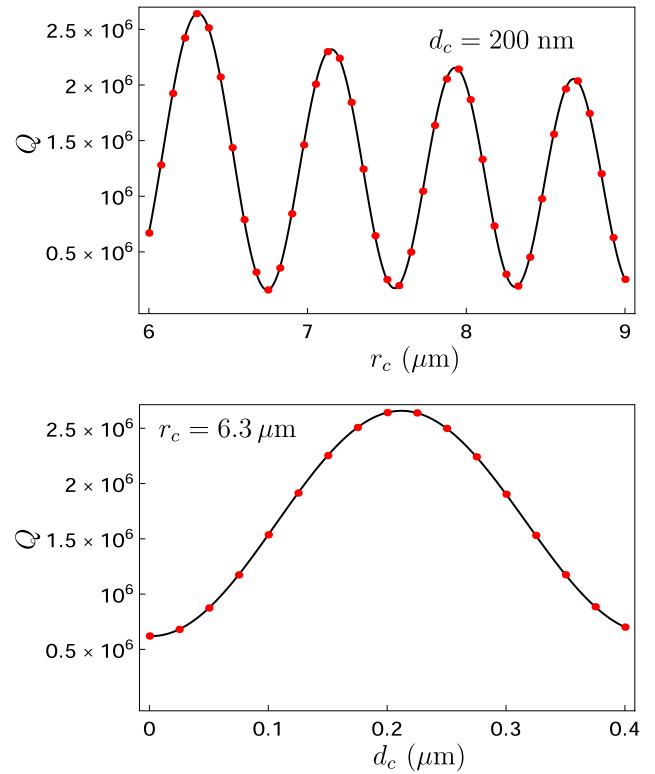
FIG. 3. The Q factor with three concentric external shells, for the same parameters as in Fig. 1. The first and second concentric shell inner radii and radial thicknesses are $(r_a, d_a) = (4.87, 0.23)\ \mu$m, $(r_b, d_b) = (5.63, 0.22)\ \mu$m, respectively. Top: Q vs the third shell inner radius r_c, with the radial thickness fixed at $d_c = 0.2\ \mu$m. Bottom: Q vs d_c, with $r_c = 6.3\ \mu$m.

index $n = 1.65$) in an air environment. Al_2O_3 has been demonstrated to be an advantageous complementary-metal-oxide-semiconductor- (CMOS) compatible host for rare-earth dopants and holds great potential for the integration of microlasers in photonic platforms [55–58]. The bare-ring cavity has inner and outer radii given by 2.5 and 3.2 μm, respectively. We focus on the fundamental radial TE mode with orbital number $\nu = 22$, which corresponds to a wavelength of $\lambda \approx 1.26\ \mu$m, in the emission band of Yb. Without a dielectric sarcophagus, $Q^c \approx 15\,000$. Adding first a single shell, Fig. 1 indicates that an eight-fold increase of Q can be obtained with an inner radius $r_a = 4.87\ \mu$m and a thickness $d_a = 0.23\ \mu$m. Next, adding a second shell with parameters $(r_b, d_b) = (5.63, 0.22)\ \mu$m, a further approximate fourfold increase is gained (see Fig. 2). Finally, another factor of 4 is obtained with a third shell with geometrical parameters given by $(r_c, d_c) = (6.3, 0.2)\ \mu$m (see Fig. 3). This brings Q to the value 2.5×10^6, which is close to the current intrinsic limit of Al_2O_3. Interestingly, Fig. 1 indicates that Q can also be significantly *decreased* for other configurations; in that case, the WGM radiation is enhanced by the external structure.

As a second example, we consider a ring cavity with an outer radius of only 1 μm and a radial thickness of 0.7 μm. We examine a resonance at $\lambda \approx 1.45\ \mu$m, that is, $\nu = 5$. Here, $Q^c = 12.3$, which is unacceptably low compared to the state of the art. The addition of five layers, of internal radii $(r_a, r_b, r_c, r_d, r_e) = (1.55, 2.22, 2.85, 3.47, 4.07)\ \mu$m and respective thicknesses $(d_a, d_b, d_c, d_d, d_e) = (0.24, 0.23, 0.23, 0.22, 0.22)\mu$m, leads to $Q = 4699$, representing and enhancement by more than a factor of 350. Figure 4 shows the change in radiation intensity and demonstrates that the mode energy stays confined in the central part of the structure. Further improvement can be obtained with additional layers. We note in this example that the optimal value of d is close to $\lambda/4n$. It is expected that d tends to that limit in the far field, as the WGMs locally tend to plane waves and the shield becomes equivalent to a Bragg reflector.

The above remark strongly suggests that the physical mechanism behind WGM-radiation shielding is a kind of Bragg reflection by the external shells. Indeed, in Fig. 5, the shells are seen to contain nearly exactly a quarter of the radial oscillation of ψ in the optimal configuration, as with plane waves [59]. There are two differences, however,
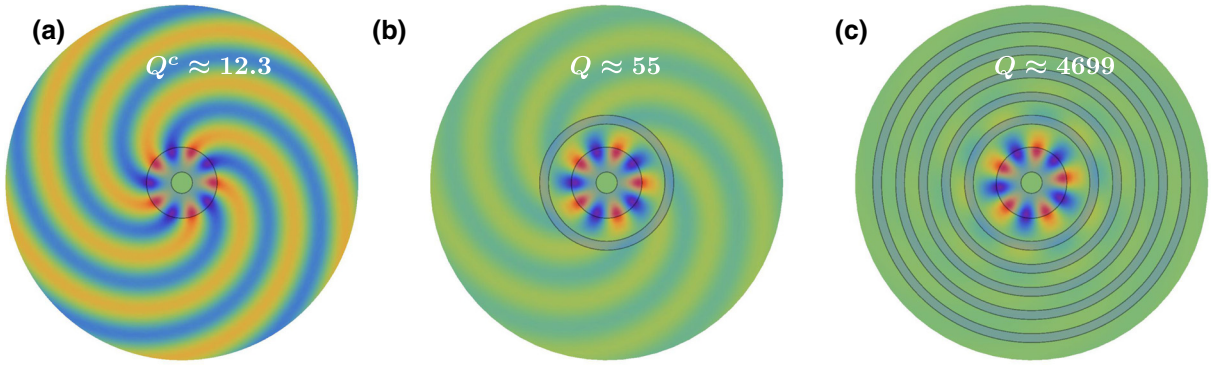
FIG. 4. The field distribution $\mathrm{Re}(\psi)$ for a TE mode with $\nu = 5$ (see text): (a) bare cavity; (b) radiation with a single shell; (c) radiation with five shells. The cavity outer radius is 1 μm.

with respect to standard Bragg reflection. First, the radial oscillations are not sinusoidal but are governed by Bessel functions. Consequently, the radiation shield is not periodic and its design rests on a formula such as Eq. (9). Second, and more fundamentally, the efficiency of the shield critically depends on where it is located—a feature that is obviously absent from standard Bragg reflection. Whereas the problem of reflection of plane waves is invariant by translation, the WGM cavity introduces an absolute reference point on the radial axis.

To illustrate this last point, let us return to the first example above, a bare Al_2O_3 cavity of external radius 3.2 μm operating on the $\nu = 22$ azimuthal mode,
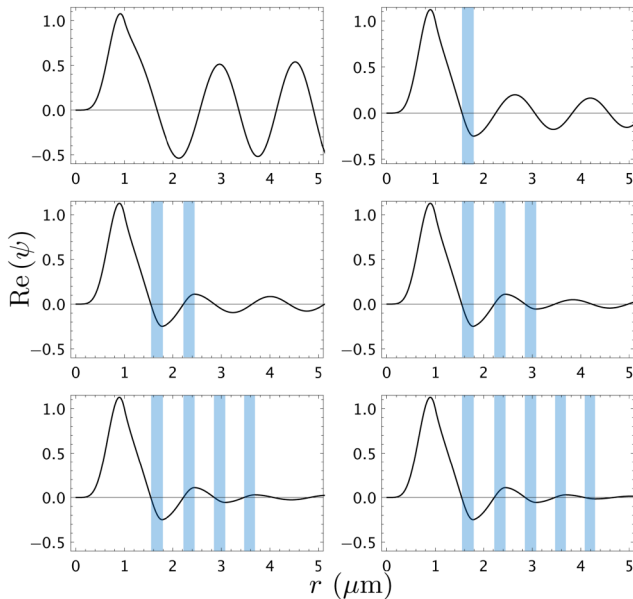
with $Q^c \approx 15\,000$. If one now encircles the cavity with two external shells with $(r_a, d_a) = (4.0, 0.15)$ μm and $(r_b, d_b) = (4.6, 0.13)$ μm, one obtains $Q \approx 215$, approximately corresponding to a 70-fold *enhancement* of the power radiated by the mode. This is also clearly visible in the radial dependence of the field shown in Fig. 6. Such a phenomenon cannot be interpreted by simply picturing the external shells as a reflector.

III. THREE-DIMENSIONAL SIMULATIONS

It is intuitively clear that, as far as radial confinement is concerned, the 2D picture provides a faithful representation of a WGM, even in three dimensions (3D). Indeed, the WGMs on a sphere with orbital number ν have a radial dependence and a characteristic equation again controlled
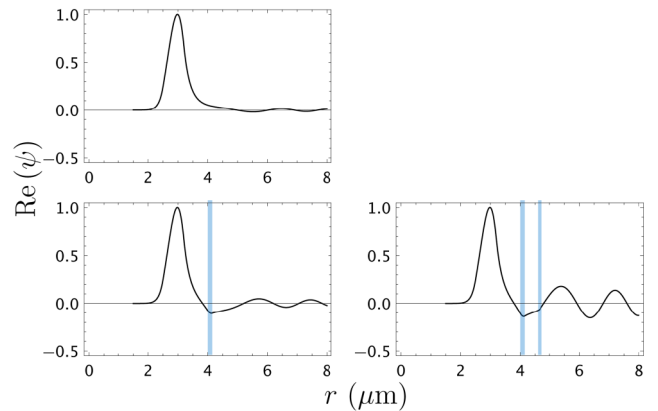

FIG. 5. The radial field distribution of the mode number $\nu = 5$ in a 1-μm-radius cavity in the absence of a shielding structure (top left) and with between one and five optimal concentric shells, depicted by the shaded regions. The field is visualized at the meridional plane $\nu\theta - kct = 0$.

FIG. 6. The radial field distribution of the mode number $\nu = 22$ for a bare-ring resonator of inner and outer radii 2.5 and 3.2 μm (the same parameters as in Fig. 1) and with one and two external concentric shells designed to enhance radiation. The external ring parameters are as follows: $(r_a, d_a) = (4.0$ μm, 0.15 μm), and $(r_b, d_d) = (4.6$ μm, 0.13 μm). The field is visualized at the meridional plane $\nu\theta - kct = 0$. Here, radiation is enhanced, with Q decreasing from the initial value of $Q^c \approx 15\,000$ to $Q \approx 215$ with two shells.
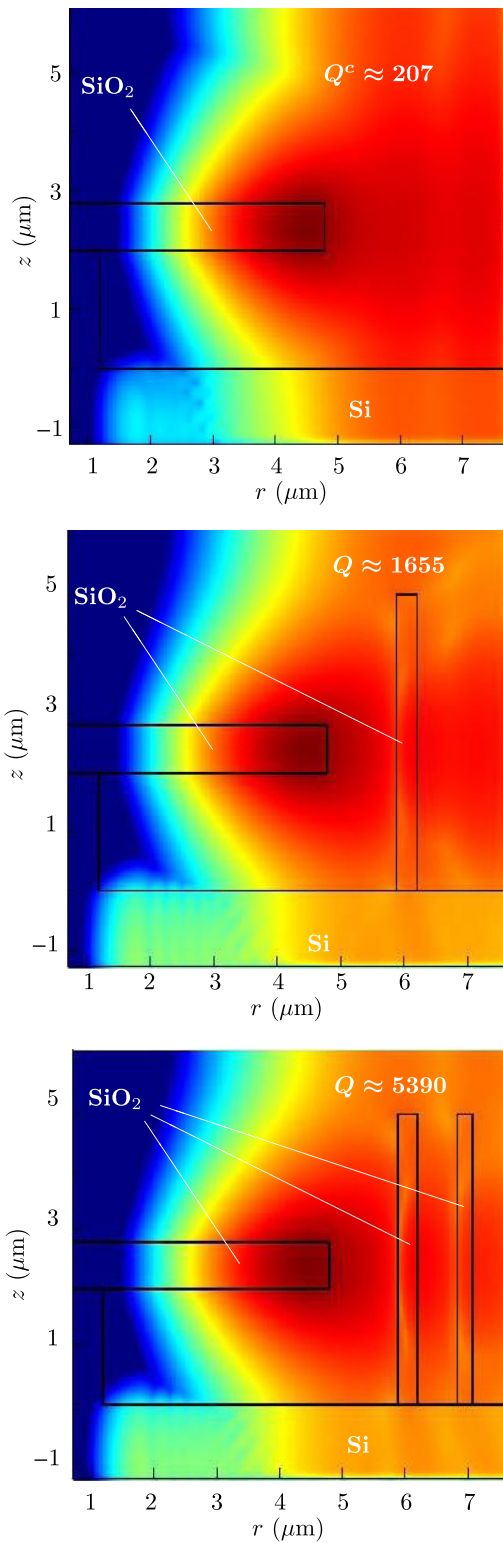
FIG. 7. The mode distribution (logarithmic color scale) of a SiO$_2$ disk cavity over a Si base. The cavity radius and thickness are 4.78 and 0.8 μm, respectively. The first shield inner radius and thickness are $r_a = 5.87$ μm and $d_a = 0.33$ μm, respectively. For the second shield, $r_b = 6.84$ μm and $d_b = 0.23$ μm. The height of both shields is 5 μm. The vacuum wavelength is 1.27 μm.
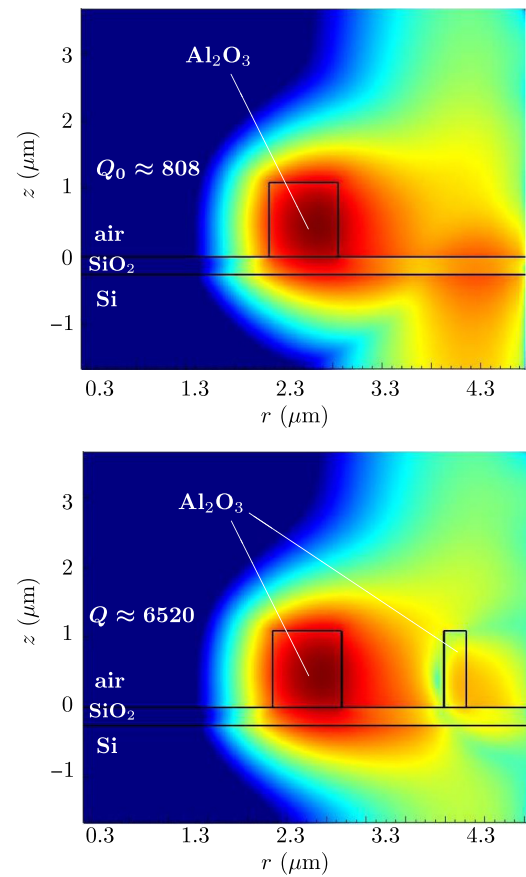

FIG. 8. The cross-section field (logarithmic color scale) of a Al$_2$O$_3$ ring made of ridge waveguides. The cavity radius, thickness, and height are 2.5, 0.7, and 1.1 μm, respectively. The base layer of SiO$_2$ is 0.25 μm thick. The shield has an inner radius and a thickness of $r_a = 3.85$ μm and $d_a = 0.23$ μm, respectively. The height of the shield is 1.1 μm. The vacuum wavelength is 1.27 μm.

by Bessel functions, albeit of order $\nu + 1/2$ instead of ν [1]. The WGMs on a sphere can thus be mapped onto those of an infinite cylinder and the two spectra coincide up to the transformation $\nu \rightarrow \nu + 1/2$. On the other hand, spherical WGMs can be strongly confined in the polar direction, with their intensity distribution confined in the immediate vicinity of the equator. Those particular WGMs are almost unaffected if the sphere is truncated along parallel planes to the equator, which, in turn, is geometrically similar to a disk. Hence, we expect that a 2D cylindrical WGM can serve as a reasonable qualitative model of WGMs in ring and disk cavities of finite vertical height and that our finding can be transposed to that case. To check this assertion, we perform 3D simulations of SiO$_2$ disk cavities on a pillar over a Si foundation, as in Fig. 7. Such a configuration, or similar ones, can be made using xenon difluoride (XeF$_2$) by etching through a silicon substrate [45]. Here again, we manage to obtain a nearly eightfold enhancement with a single external shell. With a second

external shell, the initial Q can be improved further, up to a factor of 26. This confirms both the fact that the quality factor can be increased by the design of an external shell and the fact that further enhancement can be obtained by additional shell. Hence, the gains reported in these 3D simulations should by no means be considered as ultimate values.

Finally, in Fig. 8, we confirm the effect with a ridge-waveguide ring cavity. Again, an eightfold improvement of Q is obtained with a judiciously positioned external shell. Note that the vertical confinement renders possible the excitation of the cavity in the presence of the external shells. For instance, ridge-waveguide cavities can efficiently be excited with buried waveguides [43,58]. The interaction between the buried waveguide and the concentric rings is expect to be only a small perturbation, given that the buried waveguide is only tangent to the resonator and not the outer rings. Moreover, at criticality, the buried waveguide should be designed to have a weak effect. It should yield losses that are equal to the unloaded ones, which are made small by the introduction of the concentric rings. Hence the buried waveguide should be at a sufficient distance to have an impact that is decoupled from that of the concentric rings.

IV. CONCLUSIONS

In conclusion, we devise a way to control one of the most basic limiting factors to WGM-resonator performance. With existing fabrication techniques, radiation losses can in principle be reduced to any desired degree on integrated photonic platforms. In the ratio Q/V, the quality factor could thus be limited by material factors only and not by bending losses. This could pave the way for an orders-of-magnitude improvement of performance in laser operation, sensing, or cavity-quantum-electrodynamics experiments based on WGMs.

ACKNOWLEDGMENTS

APPENDIX: TRANSFER MATRICES IN CYLINDRICAL GEOMETRY

At $r = r_{j-1}$, the continuity relations read as follows:

$$\begin{pmatrix} J_\nu(n_{j-1}x) & Y_\nu(n_{j-1}x) \\ J'_\nu(n_{j-1}x) & Y'_\nu(n_{j-1}x) \end{pmatrix} \begin{pmatrix} a_{j-1} \\ b_{j-1} \end{pmatrix}$$
$$= \begin{pmatrix} J_\nu(n_j x) & Y_\nu(n_j x) \\ y J'_\nu(n_j x) & y Y'_\nu(n_j x) \end{pmatrix} \begin{pmatrix} a_j \\ b_j \end{pmatrix}, \quad (A1)$$

where $x = kr_{j-1}$ and $y = n_j/n_{j-1}$ for TE modes or $y = n_{j-1}/n_j$ for TM modes. Inverting the matrix on the left-hand side, we obtain the following:

$$S_j = \frac{\pi n_{j-1}x}{2} \begin{pmatrix} Y'_\nu(n_{j-1}x) & -Y_\nu(n_{j-1}x) \\ -J'_\nu(n_{j-1}x) & J_\nu(n_{j-1}x) \end{pmatrix}$$
$$\times \begin{pmatrix} J_\nu(n_j x) & Y_\nu(n_j x) \\ y J'_\nu(n_j x) & y Y'_\nu(n_j x) \end{pmatrix}, \quad (A2)$$

where the first factor is the inverse of the Wronskian [54].

Consider, for instance, a simple cylinder of radius $r = R$ and index n surrounded by air. Only one transfer matrix is necessary in this case. Applying the above formula, one obtains, for a TE mode,

$$S_{22} = \frac{\pi nkR}{2} J_\nu(nkR) Y_\nu(kR) \left[\frac{Y'_\nu(kR)}{Y_\nu(kR)} - n\frac{J'_\nu(nkR)}{J_\nu(nkR)} \right]. \quad (A3)$$

The condition $S_{22} = 0$ is thus simply

$$n\frac{J'_\nu(nkR)}{J_\nu(nkR)} = \frac{Y'_\nu(kR)}{Y_\nu(kR)}, \quad (A4)$$

which is well known to give the real part of the resonances [60].

---

[1] A. B. Matsko and V. S. Ilchenko, Optical resonators with whispering-gallery modes—part I: Basics, IEEE J. Sel. Topics Quantum Electron. **12**, 3 (2006).

[2] V. S. Ilchenko and A. B. Matsko, Optical resonators with whispering gallery modes—part II: Applications, IEEE J. Sel. Topics Quantum Electron. **12**, 15 (2006).

[3] F. Vollmer and L. Yan, Label-free detection with high-Q microcavities: A review of biosensing mechanisms for integrated devices, Nanophotonics **1**, 267 (2012).

[4] W. Bogaerts, P. De Heyn, T. Van Vaerenbergh, K. De Vos, S. Kumar Selvaraja, T. Claes, P. Dumon, P. Bienstman, D. Van Thourhout, and R. Baets, Silicon microring resonators, Laser Photon. Rev. **6**, 47 (2012).

[5] Matthew R. Foreman, Jon D. Swaim, and Frank Vollmer, Whispering gallery mode sensors, Adv. Opt. Photonics **7**, 168 (2015).

[6] F. Vollmer, D. Braun, A. Libchaber, M. Khoshsima, I. Teraoka, and S. Arnold, Protein detection by optical shift of a resonant microcavity, Appl. Phys. Lett. **80**, 4057 (2002).

[7] S. Arnold, M. Khoshsima, I. Teraoka, S. Holler, and F. Vollmer, Shift of whispering-gallery modes in microspheres by protein adsorption, Opt. Lett. **28**, 272 (2003).

[8] Katrien DeVos, Irene Bartolozzi, Etienne Schacht, Peter Bienstman, and Roel Baets, Silicon-on-insulator microring resonator for sensitive and label-free biosensing, Opt. Express **15**, 7610 (2007).

[9] Adam L. Washburn, Matthew S. Luchansky, Adrienne L. Bowman, and Ryan C. Bailey, Quantitative, label-free

detection of five protein biomarkers using multiplexed arrays of silicon photonic microring resonators, Anal. Chem. **82**, 69 (2010).

[10] Muzammil Iqbal, Martin A. Gleeson, Bradley Spaugh, Frank Tybor, William G. Gunn, Michael Hochberg, Tom Baehr-Jones, Ryan C. Bailey, and L. Cary Gunn, Label-free biosensor arrays based on silicon ring resonators and high-speed optical scanning instrumentation, IEEE J. Sel. Top. Quant. Electron. **16**, 654 (2010).

[11] Matthew S. Luchansky and Ryan C. Bailey, High-Q optical sensors for chemical and biological analysis, Anal. Chem. **84**, 793 (2011).

[12] Adam L. Washburn, Winnie W. Shia, Kimberly A. Lenkeit, So-Hyun Lee, and Ryan C. Bailey, Multiplexed cancer biomarker detection using chip-integrated silicon photonic sensor arrays, Analyst **141**, 5358 (2016).

[13] F. Vollmer, S. Arnold, and D. Keng, Single virus detection from the reactive shift of a whispering-gallery mode, Proc. Natl Acad. Sci. USA **105**, 20701 (2008).

[14] T. Lu, H. Lee, T. Chen, S. Herchak, J. H. Kim, S. E. Fraser, R. C. Flagan, and K. Vahala, High sensitivity nanoparticle detection using optical microcavities, Proc. Natl Acad. Sci. USA **108**, 5976 (2011).

[15] Lina He, Şahin Kaya Özdemir, Jiangang Zhu, Woosung Kim, and Lan Yang, Detecting single viruses and nanoparticles using whispering gallery microlasers, Nat. Nanotech. **6**, 428 (2011).

[16] J. L. Dominguez-Juarez, G. Kozyreff, and J. Martorell, Whispering gallery microresonators for second harmonic light generation from a low number of small molecules, Nat. Commun. **2**, 254 (2011).

[17] G. Kozyreff, J. L. Dominguez Juarez, and J. Martorell, Non-linear optics in spheres: From second harmonic scattering to quasi-phase matched generation in whispering gallery modes, Laser Photon. Rev. **5**, 737 (2011).

[18] S. L. McCall, A. F. J. Levi, R. E. Slusher, S. J. Pearton, and R. A. Logan, Whispering-gallery mode microdisk lasers, Appl. Phys. Lett. **60**, 289 (1992).

[19] V. Sandoghdar, F. Treussart, J. Hare, V. Lefèvre-Seguin, J. M. Raimond, and S. Haroche, Very low threshold whispering-gallery-mode microsphere laser, Phys. Rev. A **54**, R1777 (1996).

[20] Kartik Srinivasan, Matthew Borselli, Oskar Painter, Andreas Stintz, and Sanjay Krishna, Cavity Q, mode volume, and lasing threshold in small diameter AlGaAs microdisks with embedded quantum dots, Opt. Express **14**, 1094 (2006).

[21] T. J. Kippenberg, S. M. Spillane, and K. J. Vahala, Kerr-Nonlinearity Optical Parametric Oscillation in an Ultrahigh-Q Toroid Microcavity, Phys. Rev. Lett. **93**, 083904 (2004).

[22] V. S. Ilchenko, A. A. Savchenkov, A. B. Matsko, and L. Maleki, Nonlinear Optics and Crystalline Whispering-Gallery Mode Cavities, Phys. Rev. Lett. **92**, 043903 (2004).

[23] H. B. Lin and A. J. Campillo, cw Nonlinear Optics in Droplet Microcavities Displaying Enhanced Gain, Phys. Rev. Lett. **73**, 2440 (1994).

[24] T. Carmon and K. J. Vahala, Visible continuous emission from a silica microphotonic device by third-harmonic generation, Nature Phys. **3**, 430 (2007).

[25] P. Del'Haye, A. Schliesser, O. Arcizet, T. Wilken, R. Holzwarth, and T. J. Kippenberg, Optical frequency comb generation from a monolithic microresonator, Nature **450**, 1214 (2007).

[26] Anatoliy A. Savchenkov, Andrey B. Matsko, Vladimir S. Ilchenko, Iouri Solomatine, David Seidel, and Lute Maleki, Tunable Optical Frequency Comb with a Crystalline Whispering Gallery Mode Resonator, Phys. Rev. Lett. **101**, 093902 (2008).

[27] Yanne K. Chembo and Nan Yu, Modal expansion approach to optical-frequency-comb generation with monolithic whispering-gallery-mode resonators, Phys. Rev. A **82**, 033801 (2010).

[28] Xu Yi, Qi-Fan Yang, Ki Youl Yang, Myoung-Gyun Suh, and Kerry Vahala, Soliton frequency comb at microwave rates in a high-Q silica microresonator, Optica **2**, 1078 (2015).

[29] G. Kozyreff, J. L. Dominguez Juarez, and Jordi Martorell, Whispering-gallery-mode phase matching for surface second-order nonlinear optical processes in spherical microresonators, Phys. Rev. A **77**, 043817 (2008).

[30] M. V. Jouravlev and G. Kurizki, Unified theory of Raman and parametric amplification in nonlinear microspheres, Phys. Rev. A **70**, 053804 (2004).

[31] J. U. Fürst, D. V. Strekalov, D. Elser, M. Lassen, U. L. Andersen, C. Marquardt, and G. Leuchs, Naturally Phase-Matched Second-Harmonic Generation in a Whispering-Gallery-Mode Resonator, Phys. Rev. Lett. **104**, 153901 (2010).

[32] J. U. Fürst, D. V. Strekalov, D. Elser, A. Aiello, U. L. Andersen, Ch. Marquardt, and G. Leuchs, Low-Threshold Optical Parametric Oscillations in a Whispering Gallery Mode Resonator, Phys. Rev. Lett. **105**, 263904 (2010).

[33] J. U. Fürst, D. V. Strekalov, D. Elser, A. Aiello, U. L. Andersen, Ch. Marquardt, and G. Leuchs, Quantum Light from a Whispering-Gallery-Mode Disk Resonator, Phys. Rev. Lett. **106**, 113901 (2011).

[34] D. W. Vernooy, A. Furusawa, N. P. Georgiades, V. S. Ilchenko, and H. J. Kimble, Cavity QED with high-Q whispering gallery modes, Phys. Rev. A **57**, R2293 (1998).

[35] E. Peter, P. Senellart, D. Martrou, A. Lemaître, J. Hours, J. M. Gérard, and J. Bloch, Exciton-Photon Strong-Coupling Regime for a Single Quantum Dot Embedded in a Microcavity, Phys. Rev. Lett. **95**, 067401 (2005).

[36] Takao Aoki, Barak Dayan, Elizabeth Wilcut, Warwick P. Bowen, A. Scott Parkins, T. J. Kippenberg, K. J. Vahala, and H. J. Kimble, Observation of strong coupling between one atom and a monolithic microresonator, Nature **443**, 671 (2006).

[37] Michael Förtsch, Josef U. Fürst, Christoffer Wittmann, Dmitry Strekalov, Andrea Aiello, Maria V. Chekhova, Christine Silberhorn, Gerd Leuchs, and Christoph Marquardt, A versatile source of single photons for quantum information processing, Nat. Commun. **4**, 1818 (2013).

[38] Şahin Kaya Özdemir, Jiangang Zhu, Lina He, and Lan Yang, Estimation of Purcell factor from mode-splitting spectra in an optical microcavity, Phys. Rev. A **83**, 033817 (2011).

[39] Anatoliy A. Savchenkov, Andrey B. Matsko, Vladimir S. Ilchenko, and Lute Maleki, Optical resonators with ten million finesse, Opt. Express **15**, 6768 (2007).

[40] Ming-Chun Tien, Jared F. Bauters, Martijn J. R. Heck, Daryl T. Spencer, Daniel J. Blumenthal, and John E. Bowers, Ultra-high quality factor planar Si_3N_4 ring resonators on Si substrates, Opt. Express **19**, 13551 (2011).

[41] Daryl T. Spencer, Jared F. Bauters, Martijn J. R. Heck, and John E. Bowers, Integrated waveguide coupled Si_3N_4 resonators in the ultrahigh-Q regime, Optica **1**, 153 (2014).

[42] B. J. M. Hausmann, I. Bulu, V. Venkataraman, P. Deotare, and M. Loncar, Diamond nonlinear photonics, Nat. Photon. **8**, 369 (2014).

[43] Zhan Su, Nanxi Li, Henry C. Frankis, E. Salih Magden, Thomas N. Adam, Gerald Leake, Douglas Coolbaugh, Jonathan D. B. Bradley, and Michael R. Watts, High-Q-factor Al_2O_3 micro-trench cavities integrated with silicon nitride waveguides on silicon, Opt. Express **26**, 11161 (2018).

[44] A. E. Shitikov, I. A. Bilenko, N. M. Kondratiev, V. E. Lobanov, A. Markosyan, and M. L. Gorodetsky, Billion Q-factor in silicon WGM resonators, Optica **5**, 1525 (2018).

[45] Ki Youl Yang, Dong Yoon Oh, Seung Hoon Lee, Qi-Fan Yang, Xu Yi, Boqiang Shen, Heming Wang, and Kerry Vahala, Bridging ultrahigh-Q devices and photonic circuits, Nature Photon. **12**, 297 (2018).

[46] G. Kozyreff and N. Acharyya, Dispersion relations and bending losses of cylindrical and spherical shells, slabs, and slot waveguides, Opt. Express **24**, 28204 (2016).

[47] Xiaohui Li, Ziyang Zhang, Shenying Qin, Tao Wang, Fangfei Liu, Min Qiu, and Yikai Su, Sensitive label-free and compact biosensor based on concentric silicon-on-insulator microring resonators, Appl. Opt. **48**, F90 (2009).

[48] Dong-Po Cai, Jyun-Hong Lu, Chii-Chang Chen, Chien-Chieh Lee, Chu-En Lin, and Ta-Jen Yen, High Q-factor microring resonator wrapped by the curved waveguide, Sci. Rep. **5**, 10078 (2015).

[49] Kiana Malmir, Hamidreza Habibiyan, and Hassan Ghafoor-ifard, An ultrasensitive optical label-free polymeric biosensor based on concentric triple microring resonators with a central microdisk resonator, Opt. Commun. **365**, 150 (2016).

[50] P. Chamorro-Posada, Q-enhanced racetrack microresonators, Opt. Commun. **387**, 70 (2017).

[51] Pedro Chamorro-Posada, Radiation in bent asymmetric coupled waveguides, arXiv:1802.04012v2.

[52] Pochi Yeh, Amnon Yariv, and Emanuel Marom, Theory of Bragg fiber, J. Opt. Soc. Am. **68**, 1196 (1978).

[53] Yong Xu, Reginald K. Lee, and Amnon Yariv, Asymptotic analysis of Bragg fibers, Opt. Lett. **25**, 1756 (2000).

[54] M. Abramowitz and I. A. Stegun, *Handbook of Mathematical Functions* (Dover, New York, 1972), 10th ed.

[55] E. H. Bernhardi, H.A.G.M. Van Wolferen, L. Agazzi, M. R. H. Khan, C. G. H. Roeloffzen, K. Wörhoff, M. Pollnau, and R. M. De Ridder, Ultra-narrow-line width, single-frequency distributed feedback waveguide laser in $Al_2O_3 : Er^3+$ on silicon, Opt. Lett. **35**, 2394 (2010).

[56] E. H. Bernhardi, H. A. G. M. van Wolferen, K. Wörhoff, R. M. De Ridder, and M. Pollnau, Highly efficient, low-threshold monolithic distributed-Bragg-reflector channel waveguide laser in $Al_2O_3 : Yb^3+$, Opt. Lett. **36**, 603 (2011).

[57] E. H. Bernhardi, M. R. H. Khan, C. G. H. Roeloffzen, H. A. G. M. van Wolferen, K. Wörhoff, R. M. De Ridder, and M. Pollnau, Photonic generation of stable microwave signals from a dual-wavelength $Al_2O_3 : Yb^3+$ distributed-feedback waveguide laser, Opt. Lett. **37**, 181 (2012).

[58] Henry C. Frankis, Zhan Su, Nanxi Li, Emir Salih Magden, Mengyuan Ye, Michael R. Watts, and Jonathan D. B. Bradley, in *CLEO: Science and Innovations* (Optical Society of America, 2018), pp. STh3I–3.

[59] Emil Wolf and Max Born, *Principles of Optics: Electromagnetic Theory of Propagation Interference and Diffraction of Light* (Butterworth-Heinemann, Oxford, 1980).

[60] C. C. Lam, P. T. Leung, and K. Young, Explicit asymptotic formulas for the positions, widths, and strengths of resonances in Mie scattering, J. Opt. Soc. Am. B **9**, 1585 (1992).